



# The pyridazine–tetrathiafulvalene conjugates: synthesis, photophysical, and electrochemical properties

Ningjuan Zheng<sup>a</sup>, Bao Li<sup>b</sup>, Changwei Ma<sup>a</sup>, Tie Chen<sup>a</sup>, Yuhe Kan<sup>c,\*</sup>, Bingzhu Yin<sup>a,\*</sup>

<sup>a</sup>Key Laboratory of Natural Resources of Changbai Mountain & Functional Molecules, Yanbian University, Ministry of Education, Yanji, Jilin 133002, PR China

<sup>b</sup>State Key Laboratory of Supramolecular Structure and Materials, College of Chemistry, Jilin University, Changchun 130012, PR China

<sup>c</sup>Jiangsu Key Laboratory for Chemistry of Low-Dimensional Materials, Huaiyin Teachers College, Huaiyin 223300, PR China

## ARTICLE INFO

### Article history:

Received 6 October 2011

Received in revised form 8 December 2011

Accepted 13 December 2011

Available online 16 December 2011

### Keywords:

Tetrathiafulvalene

Pyridazine

Donor–acceptor conjugate

Charge transfer

Photophysical property

Electrochemical behavior

## ABSTRACT

To study the electronic interactions in donor–acceptor (D–A) conjugates as a precursor of optoelectronic materials, a series monopyridazine-annulated tetrathiafulvalenes and a bispyridazine-annulated tetrathiafulvalene were synthesized by a condensation reaction of 2,3-dimethoxycarbonyl-6,7-dibutylthiotetrathiafulvalene or/and 2,3,6,7-tetramethoxycarbonyltetrathiafulvalene with hydrazine hydrate and structurally characterized by conventional chemical and physical methods. Their electronic properties have been studied experimentally by the combination of electrochemistry and UV–vis spectroscopy. All of monopyridazine–tetrathiafulvalene conjugates **7–13** show intramolecular charge transfer interaction in ground states, which is rationalized on the basis of density functional theory. Their HOMO energy levels and  $E_g^{\text{opt}}$  values were estimated to be  $-4.88$  to  $-5.07$  eV from cyclic voltammetry and  $2.43$ – $2.79$  eV from the absorption spectra, respectively. The X-ray crystallographic analyses of the pyridazine–tetrathiafulvalene conjugates **7**, **11–13** are also reported.

© 2011 Elsevier Ltd. All rights reserved.

## 1. Introduction

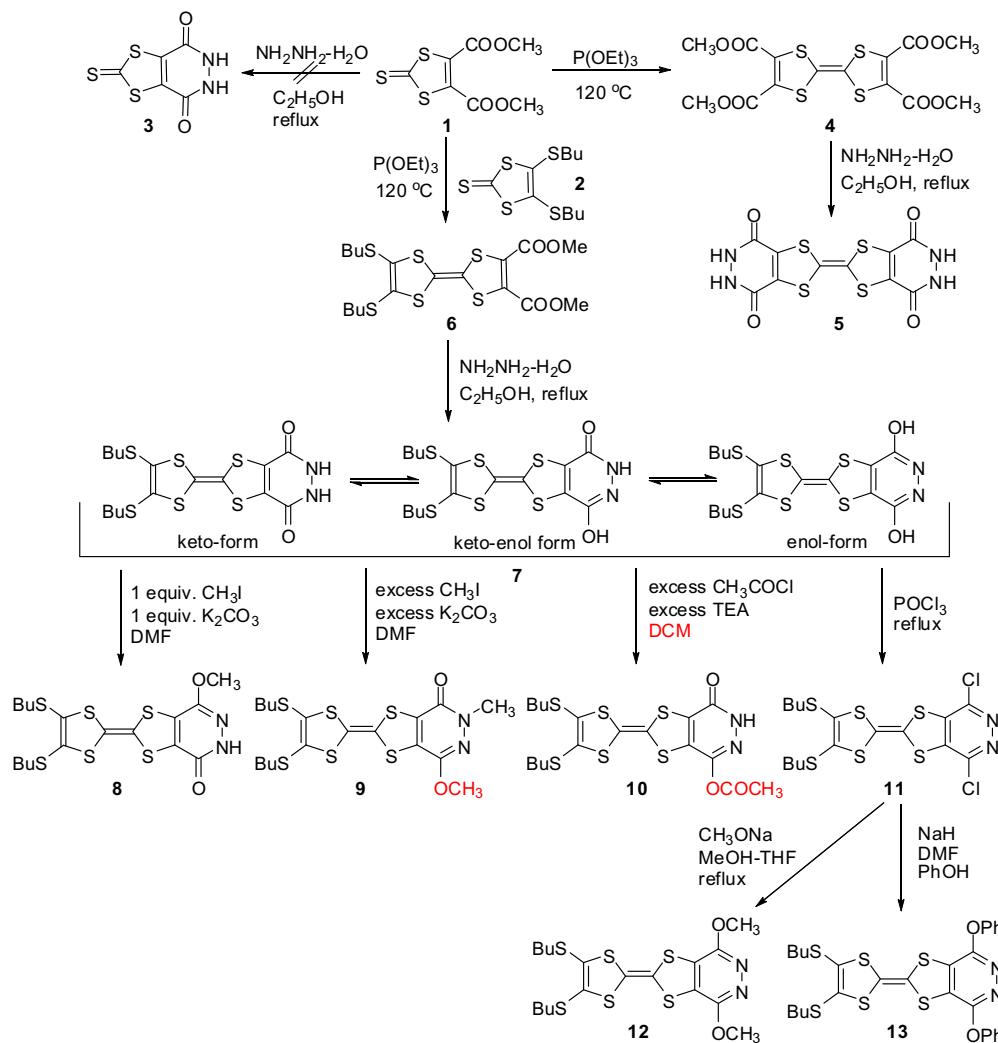
Among the various candidates of organic materials for optoelectronic applications,<sup>1</sup> tetrathiafulvalene (TTF) is most attractive due to its excellent electron-donating properties. The optoelectronic properties of these materials are clearly dependent on both the molecular structure and architecture in the solid state and so the TTF skeleton and peripheral substitutes has been extensively modified in order to enhance dimensionality of the materials and/or to achieve a suitable solid-state organization.<sup>2</sup> Additionally, because of the strong electron-donating property of TTF, its derivatives are usually sensitive to air and light, which is one of the main drawbacks of TTF for practical applications. In order to overcome this barrier, heterocycle has been annulated to decrease its HOMO energy level, which suitable for *P*-type organic semiconductors.<sup>3</sup> A variety of donor molecules have been synthesized in which the TTF core is annulated to benzenoid, furan, thiophene, selenophene, pyrimidine or pyrazine units; all of these compounds have oxidation potentials appreciably higher than that of TTF itself.<sup>3,4</sup> Among the heterocyclic-fused TTF donors, the pyrazine-annulated TTF derivatives showed the excellent *P*-type FET (field effect transistor) performances in thin films. Annulation of pyrazine

rings to the TTF skeleton was effective to enhance the intermolecular interaction, which was also useful to enhance the stability of the FET device to oxygen.<sup>3</sup> Another heterocyclic-fused TTFs, the pyrimidine-fused TTF derivatives have a unique ability to form unusual stable cation radical intermolecular salts (betaines). These cation radical salts and betaines in pressed pellets showed an unexpectedly low resistivity and semiconductor behavior with low values of activation energy.<sup>4i,j</sup> As early as in 1983, a bispyridazinoTTF has been synthesized by condensation of tetraformyl-TTF with excess hydrazine hydrate and its  $\pi$ -donor ability has also been reported.<sup>5</sup> Surprisingly, to the best of our knowledge, there is no any report on exploring the optoelectronic applications of pyridazine-annulated TTFs in detail. It is probably due to the poor solubility in organic solvents and an absence of available substitutes. Keeping this information in mind, we annulated a pyridazine ring to one side of TTF skeleton to synthesize a series of monopyridazinoTTF derivatives as shown in **Scheme 1**. Most of the TTF derivatives are soluble in chloroform, methylene chloride, ethyl acetate, tetrahydrofuran, dimethyl sulfoxide, and acetone and slightly soluble in acetonitrile except for the keto-forms **7** and **5**. In the present work, we describe the synthesis, photophysical and electrochemical properties of the monopyridazinoTTF derivatives. The X-ray crystallographic analyses of **7**, **11–13**, together with preliminary formation of a charge transfer complex between the donor **13** with nitrosonium

\* Corresponding authors. Tel.: +86 433 2732298; fax: +86 433 2732456; e-mail address: [zqcong@ybu.edu.cn](mailto:zqcong@ybu.edu.cn) (B. Yin).

hexafluorophosphate (NOPF<sub>6</sub>), are also reported. Such systems are of prime interest due to the excellent solubility in organic solvents and diversified functionalization.

dithiole-2-one in net triethyl phosphite to give an unsymmetrical diester derivative of TTF (6). Fortunately, the diester 6 reacted with hydrazine hydrate in refluxing ethanol to give a soluble keto-form 7



Scheme 1. Synthesis route to the pyridazinoTTF derivatives.

## 2. Results and discussion

### 2.1. Syntheses and crystal structure analysis

The standard method of synthesis of the pyridazine ring is the action of hydrazine on 1,4-dicarbonyl compounds or their equivalent.<sup>6</sup> We once attempted to obtain the pyridazine derivative (3) by the reaction of dimethyl 2-thioxo-1,3-dithiole-4,5-dicarboxylate (1) with hydrazine hydrate, but the experiment is unsuccessful (Scheme 1). Self-coupling reaction of compound 1 in net triethyl phosphite gave 2,3,6,7-tetramethoxycarbonyl TTF (4), then 4 condenses with hydrazine hydrate to give a bispyridazine-annulated TTF 5 in good yield. Molecular structure of the bispyridazine-annulated TTF 5 has been presumed by mass and IR spectral studies. The mass spectrum of compound 5 displays the parent ion peak at  $m/z$  371.0, corresponding to  $[M-H]^-$  (370.9) of 5 (Fig. S1). The FT-IR spectrum of 5 moreover exhibits only a strong absorption peak of carbonyl at  $1658\text{ cm}^{-1}$  and a weak absorption peak of amide at  $3182\text{ cm}^{-1}$  (Fig. S2a). Unfortunately the structure and properties of compound 5 are impossible to be fully investigated owing to its extreme insolubility. Cross-coupling of 1 with 4,5-dibutylthio-1,3-

in a moderate yield. Upon addition of 1 equiv methyl iodide, 7 was subjected to the methylation to afford a keto–enol form monomethyl ether 8 in a good yield. As we expected, the reaction of keto-form 7 with an excess methyl iodide in DMF at room temperature leads to an *N,O*-dimethyl keto–enol form derivatives 9 in high yield. Unexpectedly, 7 reacted with an excess acetyl chloride in the presence of triethylamine to give only an *O*-monoacyl keto–enol form derivatives 10. The key intermediate dichloropyridazinoTTF 11 was easily synthesized starting from 7 with refluxing POCl<sub>3</sub> in 90% yield. The *O,O*-dimethyl enol-form derivatives 12 was prepared by nucleophilic substitution of 11 with sodium methoxide in a mixture of MeOH and THF (2:1, v/v) in 48% yield. Similarly, the condensation reaction of 11 with phenoxide in DMF gives rise to an *O,O*-diphenolated enol-form derivatives 13 in a good yield. The data of the elemental and MALDI-TOF mass analyses are consistent with the constituents of the proposed pyridazinoTTF derivatives 5–13 (see Supplementary data). Theoretically, compound 7 is likely to exist as an equilibrium of three tautomeric forms as shown in Scheme 1. Both <sup>1</sup>H and <sup>13</sup>C NMR spectra indicate that compounds 7, 11–13 all exist in the C<sub>2</sub>-symmetrical structures, in which only the FT-IR spectra of 7 exhibits a strong absorption peak of carbonyl of

amide at  $1647\text{ cm}^{-1}$  (Fig. S2b, f–h). Therefore **7** could be assigned as the keto-form, while **11–13** could be assigned as the enol-form derivatives, respectively. In contrast, compounds **8–10** showed the non  $C_2$ -symmetrical structures in both  $^1\text{H}$  and  $^{13}\text{C}$  NMR spectra. Furthermore, in  $\text{CDCl}_3$  the  $^1\text{H}$  NMR spectra of **8** and **10** consists of a singlet peak at  $\delta$  3.89 and 2.34 ppm, respectively, which are characteristic for the methyls in the methoxy group and acetyl group, respectively. The  $^1\text{H}$  NMR spectrum of **9** shows two methyl peaks at 3.87 and 3.65 ppm, which could be assigned as an *O*-methyl group and a *N*-methyl group, respectively. Of them, the FT-IR spectra of **8** and **9** exhibit only one strong absorption peak of amide carbonyl at  $1653$  and  $1647\text{ cm}^{-1}$ , respectively, while **10** exhibits an absorption peak of amide carbonyl at  $1651\text{ cm}^{-1}$  and an absorption peak of ester carbonyl at  $1778\text{ cm}^{-1}$  (Fig. S2c–e). In view of the facts mentioned above, the compounds **8–10** could be assigned as *O*-methyl, *O,N*-dimethyl, and *O*-acetyl substituted keto–enol form derivatives, respectively.

Crystals suitable for an X-ray diffraction study have been obtained for compounds **7**, **11–13** through recrystallization from DMF for **7** and from hexane for **11–13**. Their molecular structures and crystal data are shown in Fig. 1 and Table 1. The asymmetric unit of compound **7** is composed of two molecules (**7A** and **7B**) and one ethanol molecule (Fig. 1a). The rigid components of both **7A** and **7B** exhibit 'boat' conformations as often observed with neutral TTF. For **7A**, the dihedral angle of two parts (one is composed of N1, N2, C1 to C4, O1, O2, S1, and S2, and the other one is composed of S3 to S6, C7, and C8) is  $33.77(19)^\circ$ . For **7B**, the dihedral of two parts is  $22.45(13)^\circ$  (one is composed of N3, N4, C17 to C20, O3, O4, S7, and S8, and the other is composed of S9 to S12, C23, and C24). Furthermore, in the same asymmetric unit, the two 'boat' conformation parts arrange in the style of back-to-back. Another difference of **7A** and **7B** molecules is the extension direction of butyls. For **7A**, the two butyls extend to

**Table 1**  
Crystal data and structure refinement of complexes **7**, **11–13**

Compd	<b>7</b>	<b>11</b>	<b>12</b>	<b>13</b>
Formula weight	975.44	501.58	492.75	616.88
Temperature (K)	293(2)	296(2)	296(2)	296(2)
$\lambda$ (Å)	0.71073	0.71073	0.71073	0.71073
Crystal system	Triclinic	Triclinic	Orthorhombic	Triclinic
Space group	<i>P</i> -1	<i>P</i> -1	<i>Pbcn</i>	<i>P</i> -1
<i>a</i> (Å)	10.383(2)	7.671(6)	19.376(3)	9.169(2)
<i>b</i> (Å)	12.607(3)	11.215(8)	10.578(6)	10.852(2)
<i>c</i> (Å)	18.296(4)	13.310(11)	23.124(6)	15.292(3)
$\alpha$ (deg)	93.64(3)	86.10(3)	90	96.86(3)
$\beta$ (deg)	101.43(3)	79.57(3)	90	94.78(3)
$\gamma$ (deg)	110.38(3)	79.27(2)	90	91.28(3)
Volume (Å <sup>3</sup> )	2177.5(8)	1105.9(2)	4739.0(3)	1504.6(5)
<i>Z</i>	2	2	8	2
$D_{\text{calcd}}$ (g/cm <sup>3</sup> )	1.488	1.506	1.381	1.362
Abs coeff. (mm <sup>-1</sup> )	0.647	0.865	0.594	0.483
$R_{\text{int}}$	0.0210	0.0476	0.0381	0.0229
$R$ (000)	1012	516	2064	644
GOF on $F^2$	1.126	1.051	1.067	1.112
$R$ [ $I > 2\sigma(I)$ ] <sup>a</sup>	0.0601	0.0507	0.0522	0.0477
$R_w$ (all data) <sup>b</sup>	0.1863	0.1254	0.1580	0.1292
(Residues) <sub>max</sub> (e/Å <sup>3</sup> )	0.844	0.453	0.560	0.686
(Residues) <sub>min</sub> (e/Å <sup>3</sup> )	-0.648	-0.489	-0.289	-0.396

<sup>a</sup>  $R = \frac{\sum |F_o| - \sum |F_c|}{\sum |F_o|}$ .

<sup>b</sup>  $R_w = \left[ \frac{\sum w(F_o^2 - F_c^2)^2}{\sum w(F_o^2)^2} \right]^{1/2}$ .

the two side of the plane formed by S3–S6, while for **7B**, the two butyls nearly lie on the same plane with one formed by S9 to S12. In the crystal structure of **7**, both **7A** and **7B** are in diketone form, which can also be confirmed by NMR and IR. For **7A**, the distances of C1, O2, and C4, O1 are  $1.227(3)\text{ \AA}$  and  $1.198(3)\text{ \AA}$ , respectively, showing the existence of C=O. In addition, the bond lengths of C1–N2, N2–N1, and N1–C4 are  $1.254(4)\text{ \AA}$ ,  $1.317(3)\text{ \AA}$ , and  $1.320(3)\text{ \AA}$ ,

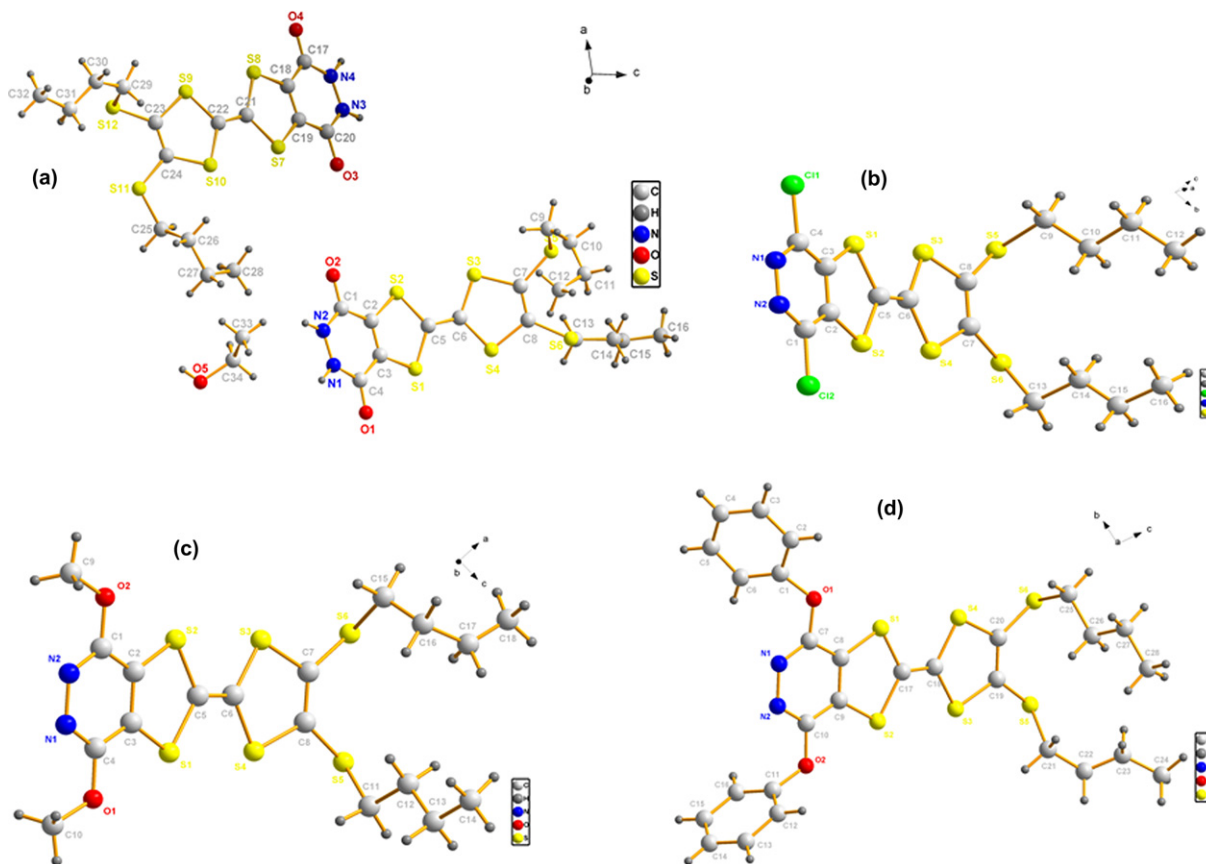


**Fig. 1.** Molecular structures of pyrazinoTTFs **7** (a), **11** (b), **12** (c), and **13** (d).

respectively, showing the single C–N bonds and N–N bonds. The bond lengths of **7B** are similar with one of **7A**. In the crystal structure of compound **7A**, the intermolecular N–H···O (N3–H3···O2,  $x_1$   $x_2$ :  $x, -1+y, z$ ; N4–H4···O1,  $x_2$   $x_3$ :  $1+x, 1+y, z$ ) hydrogen bonds with the distances of H···O of 2.461 (6) Å and 1.890 (5) Å link the molecules to form an infinite chain along [001] direction. Different with compound **7**, there is only one molecule in the asymmetric unit for compounds **11–13**. In addition, except for butyls, all the other non-hydrogen atoms nearly lie on the same plan and all butyls in the three compounds lie on the same side of the plan. Due to the absence of C=O in the six-membered heterocycle, there are some differences for neighboring C–N and N–N bond lengths comparing with complex **7**. For compound **11**, the C–N and N–N bond lengths are 1.304 (5) Å, 1.314 (5) Å, and 1.336 (4) Å, respectively, which are longer than one in compound **7**. For compound **12**, the C–O bond lengths are 1.346 (4) Å and 1.348 (4) Å, which are much longer than one of compound **7** with the distance of C–O of 1.227 (3) Å and 1.198 (3) Å, showing the single bonds between C and O atoms. For compound **13**, the C–O bond lengths are 1.359 (3) Å and 1.366 (3) Å, which is comparable with one of compound **12**, also showing the existence of single bond between C and O atoms. In compound **13**, two benzene rings exhibit different dihedral angles with TTF core plan, one is 53.44 (11)° and the other is 84.05 (16)°. For all of compounds **11–13**, there are no obvious hydrogen bonds or  $\pi$ – $\pi$  interactions in the crystal structure.

## 2.2. Photophysical and electrochemical properties

To fit the energetic scheme of the organic optoelectronic materials, it is necessary to determine the energy levels of the highest occupied molecular orbital (HOMO) and lowest unoccupied molecular orbital (LUMO) and the width of the gap between the bands of each component through electrochemistry.<sup>7</sup> The energy gap between the bands can moreover be easily determined with the absorption spectroscopy.<sup>8</sup>

The absorption spectra of **7–13** dissolved in CHCl<sub>3</sub> ( $5 \times 10^{-5}$  M) are presented in Fig. 2a. They show a very weak and broad absorption band, whose highest point was located around 420 nm and an intense absorption band centered around 320 nm, respectively. The absorption bands centered around 420 nm result from an ICT transition from the TTF unit to the substituted pyridazine moieties. In the UV region, the strong absorption bands are characteristic for  $\pi$ – $\pi^*$  transitions located on both, the TTF and the substituted pyridazine subunits.<sup>9</sup> The absorption maxima,  $\lambda_{\text{maxUV}}$ , the values of 10% of the absorption maximum taken from the lower energy side,  $\lambda_{10\% \text{ max}}$ , and the optical band gap energies,  $E_{\text{g}}^{\text{opt}}$ , are given in Table 2. As can be seen in Table 2, the optical band gap energy,  $E_{\text{g}}^{\text{opt}}$ , of pyridazinoTTFs **7–13** was estimated to be about 2.43–2.79 eV.<sup>8</sup> It is surprising that the number and kind of the substituting groups at pyridazine ring do not nearly influence the wavelength of  $\pi$ – $\pi^*$  transition, but influence slightly the ICT transition and the optical band gap energies,  $E_{\text{g}}^{\text{opt}}$ , of pyridazinoTTFs.

To investigate the electron-donating properties of synthesized pyridazinoTTFs, chemical oxidation of **13** in CHCl<sub>3</sub> solution ( $5 \times 10^{-5}$  M) was conducted with an excess TCNQ in CHCl<sub>3</sub> solution (Fig. S3). But no CT band was observed in the 400–1000 nm region, which might be attributed to the presence of the electron-withdrawing pyridazine ring. Whereas, upon 0.5 equiv of NOPF<sub>6</sub> to a CHCl<sub>3</sub> solution of **13** ( $5 \times 10^{-5}$  M) resulted in the decreasing of the absorption band around 319 nm, and the concomitant emergence of new absorption bands characteristic for the formation of the cation-radical species around 380 nm (Fig. 2b). Upon successive addition of aliquots of NOPF<sub>6</sub>, the new absorption band at 380 nm progressively increases and red-shifts to 402 nm, while the main band at 319 nm continuously decreases, but no further changes occurred after the addition of 1.5 equiv of NOPF<sub>6</sub>.

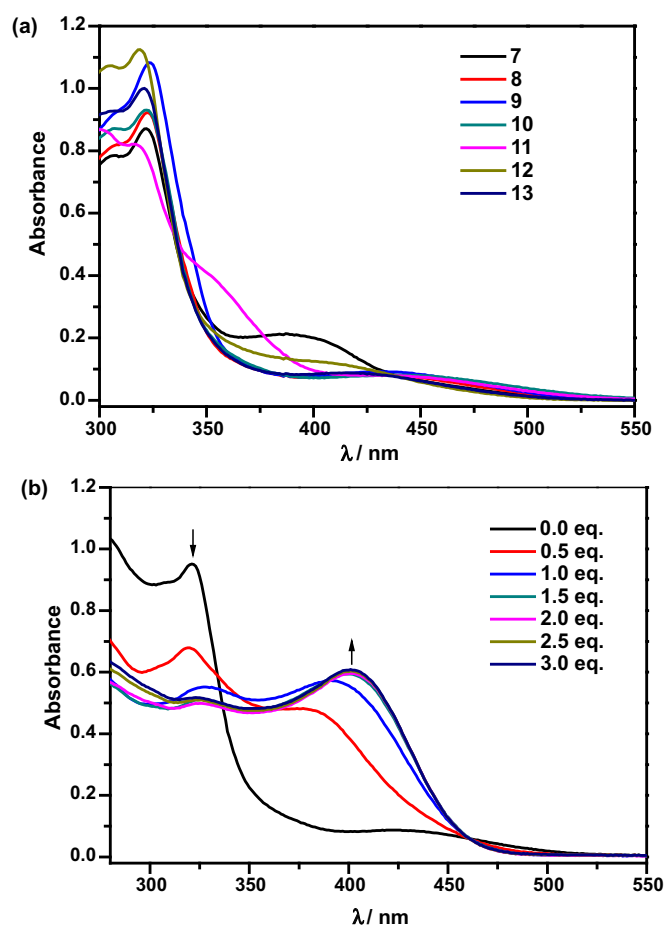


Fig. 2. (a) UV–vis absorption spectra in  $5 \times 10^{-5}$  M CHCl<sub>3</sub> solution of the pyridazinoTTFs **7–13**. (b) Variation of the UV–vis absorption spectra of **13** in  $5 \times 10^{-5}$  M CHCl<sub>3</sub> solution upon successive addition of aliquots of NOPF<sub>6</sub>.

Table 2

UV–vis absorption spectroscopy data,  $E_{\text{g}}^{\text{opt}}$ , redox potentials (vs Ag/AgCl), and HOMO energies obtained from cyclic voltammetry for pyridazinoTTF **7–13**

Compd	$\lambda_{\text{max, UV}}/\text{nm}$	$\lambda_{10\% \text{ max}}/\text{nm}$	$E_{\text{g}}^{\text{opt}}/\text{eV}^{\text{a}}$	$E_{1/2}^{\text{red}}/\text{V}$	$E_{\text{onset}}^{\text{red}}/\text{V}$	$E^{\text{HOMO}}/\text{eV}^{\text{b}}$	$E^{\text{LUMO}}/\text{eV}^{\text{c}}$
<b>7</b> <sup>e</sup>	387	458	2.79	0.743 <sup>d</sup>	0.643	−5.03	−2.24
<b>8</b>	430	520	2.45	0.537	0.465	−4.88	−2.43
<b>9</b>	432	518	2.46	0.525	0.465	−4.88	−2.42
<b>10</b>	443	545	2.35	0.628	0.559	−4.96	−2.61
<b>11</b>	432	526	2.43	0.734	0.671	−5.07	−2.64
<b>12</b>	425	501	2.55	0.703	0.645	−5.05	−2.45
<b>13</b>	410	491	2.60	0.590	0.524	−4.92	−2.36

<sup>a</sup> Optical band gap according UV–vis absorption (onset method).  $E_{\text{g}}^{\text{opt}}(10\%) = hc/\lambda_{10\% \text{ max}}$  [Ref. 8].

<sup>b</sup> Energy level of highest occupied molecular orbital according cyclovoltammetry.  $E^{\text{HOMO}}/E^{\text{LUMO}} = [-(E_{\text{onset}}^{\text{red}} - 0.45) - 4.8]$  eV, where the value 0.45 V for ferrocene versus Ag/Ag+ and 4.8 eV the energy level of ferrocene below the vacuum [Ref. 8].

<sup>c</sup> The LUMO levels were estimated from the HOMO–LUMO energy gaps, which were obtained from the absorption onset since their reduction potential could not be observed.

<sup>d</sup> 0.743 is the  $E_{\text{pa}}^1$  value because of the first redox of **7** is irreversible.

<sup>e</sup> The CV and DPV measurement of compound **7** was performed in dry DMSO.

Cyclic voltammetry (CV) and/or differential pulse voltammetry (DPV) are easy and effective methods to measure redox potentials and to simultaneously evaluate both the HOMO and LUMO energy levels and the band gap energy,  $E_{\text{g}}^{\text{cc}}$ , of an organic molecule. To evaluate the electron-donating properties and the HOMO energy levels of pyridazinoTTFs, the CV (Table 2 and Fig. 3) and DPV (Fig. S4) measurements were performed in a mixture of dry dichloromethane and acetonitrile (1:1) at room temperature. As

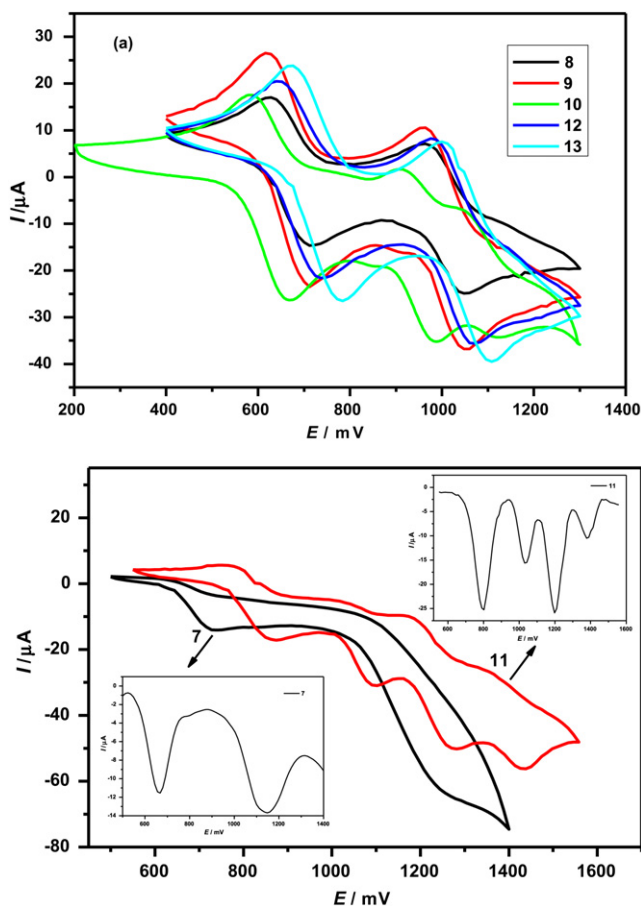


**Fig. 3.** Cyclic voltammograms of **8–10**, **12–13** (a) and **7**, **11** (b) in  $\text{CH}_2\text{Cl}_2/\text{MeCN}$  (1:1) ( $1 \times 10^{-3}$  M). Inset: differential pulse voltammogram of compound **7** (bottom) and **11** (top) in  $\text{CH}_2\text{Cl}_2/\text{MeCN}$  (1:1) ( $1 \times 10^{-3}$  M).

anticipated from its structure, all of monopyridazinoTTFs exhibit two reversible one-electron redox couples with the exception of the non-substituted pyrazinoTTF **7** and the dichloro-substituted pyrazinoTTF **11**, which are associated with the successive oxidation of the TTF unit to  $\text{TTF}^{\cdot+}$  and  $\text{TTF}^{2+}$ , respectively (Fig. 3). In comparison to TTF ( $E_{1/2}^1=0.34$  V,  $E_{1/2}^2=0.73$  V),<sup>10</sup> their oxidation potentials are positively shifted by 190–400 mV owing to the annulation of electron-withdrawing pyridazine ring. Compounds **8** and **9** exhibit typical two reversible oxidation waves with half-wave potentials ( $E_{1/2}$ ) at  $\sim 0.537$  and  $0.879$  V, while compounds **10**, **12**, and **13** showed split second redox couples, with  $E_{1/2}^2$  at  $\sim 0.999$  V and  $\sim 1.208$  V, which probably is caused by adsorption phenomena on the electrode<sup>11</sup> (Fig. 3a). In contrast, CV analysis of **7** displays two irreversible oxidation waves at  $E_{pa}^1=0.662$ ,  $E_{pa}^2=1.144$  V (Fig. 3b). Compound **11** containing two chlorine atoms displays a complicated cyclic voltammogram, which showed four irreversible one-electron oxidations at 0.799, 1.031, 1.199, and 1.379 V, respectively (Fig. 3b). Obviously, the presence of the different substituents at the pyridazine ring has a strong influence on the electron-donating ability of TTF. It is noticeable that introduction of chlorine atom probably induced the degradation of pyridazinoTTF system. The redox potentials,  $E_{1/2}^n/\text{V}$ , the onset potentials,  $E^{\text{onset}/\text{ec}}/\text{V}$ , and HOMO energies,  $E^{\text{HOMO}}/\text{eV}$ , obtained from cyclic voltammetry for PyridazinoTTF **7–13** are listed in Table 2. As shown in Table 2, their HOMO levels were estimated from the onset of oxidation potentials to be between  $-4.88$  and  $-5.07$  eV. HOMO levels of good *P*-type organic semiconductors are known typically to be in the range of  $-4.9$  to  $-5.5$  eV.<sup>12</sup> Clearly, such a combination of multi-redox property of the TTF moiety and strong electron-withdrawing

ability of the pyridazine part may provide low HOMO energy levels and large energy gaps to improve its air/light stability,<sup>13</sup> which suggest that the pyridazine-TTF conjugates are promising hole transporting organic materials.

To investigate the nature of the electronic transitions that give rise to the absorption bands observed in the electronic spectra, the lowest-energy singlet excited states were calculated for compound **12** using the time-dependent DFT (TDDFT) approach (see Supplementary data). The results of the TD-DFT calculations performed with the B3LYP, PBE0, BH and HLYP, and MPWPW91 functionals in chloroform solvent are shown in Fig. 4. The excitation energies, oscillator strengths, and transition characters are listed in Table 3.

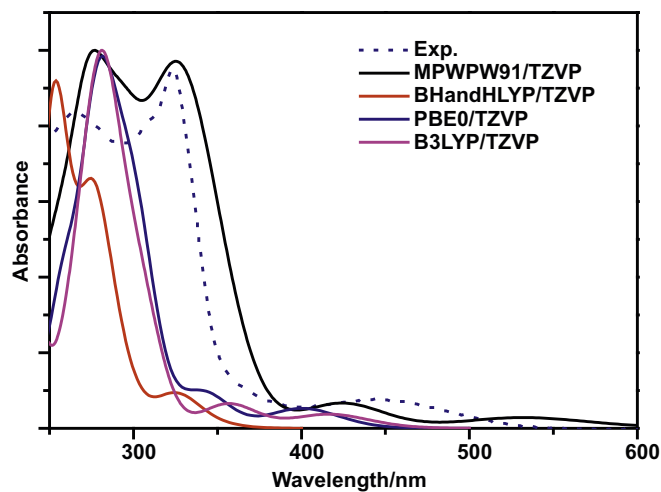


**Fig. 4.** Comparison between experimental (dot) and simulated electronic absorption spectra of compound **12** at MPWPW91/TZVP level in chloroform solvent.

**Table 3**

MPWPW91/TZVP calculated absorption wavelength ( $\lambda$ , in nm), transition energies ( $\Delta E$ , in eV), oscillator strength ( $f$ ), and major transition contribution for **12** in chloroform

State	$\lambda_{\text{cal}}$	$\Delta E/\text{eV}$	$f$	Transition nature
$S_1$	534.0	2.32	0.0116	HOMO $\rightarrow$ LUMO (99%)
$S_2$	491.0	2.53	0.0011	HOMO $\rightarrow$ LUMO+1 (100%)
$S_3$	425.1	2.92	0.0279	HOMO $\rightarrow$ LUMO+2 (95%)
$S_7$	350.4	3.54	0.1121	HOMO $\rightarrow$ LUMO+3 (27%)
$S_{12}$	333.4	3.72	0.1873	HOMO $\rightarrow$ LUMO+4 (61%)
				HOMO $\rightarrow$ LUMO+3 (38%)
				HOMO $\rightarrow$ LUMO+4 (20%)
				HOMO $\rightarrow$ LUMO+6 (32%)

MPWPW91 provides transition wavelengths and band shape in better agreement with experimental data than other functionals. MPWPW91 calculations predict that the long wavelength absorption bands observed for **12** at 425 nm is due to electronic transitions to the first three excited singlets,  $S_1$  to  $S_3$ , calculated at 2.32–2.92 eV. The  $S_1$  state results from the HOMO  $\rightarrow$  LUMO excitation (Fig. 5), which is assigned as charge transfer from TTF to pyridazine moiety. The  $S_3$  state originates in the HOMO  $\rightarrow$  LUMO+2 excitation, and corresponds to an electron excitation from TTF to sulfur atoms in dibutyl and TTF moiety. Therefore, calculations confirm the charge transfer (CT) nature of the low-energy absorption bands of **12**. For the excited states at the intense absorption intensity is 333 nm, and mainly corresponds to  $S_{12}$  state electron excitation from HOMO-2 to LUMO+3, which are assigned as charge transfer from pyridazine ligand to TTF. Moreover, the absorption property of the molecule in DMSO is same to that in chloroform.

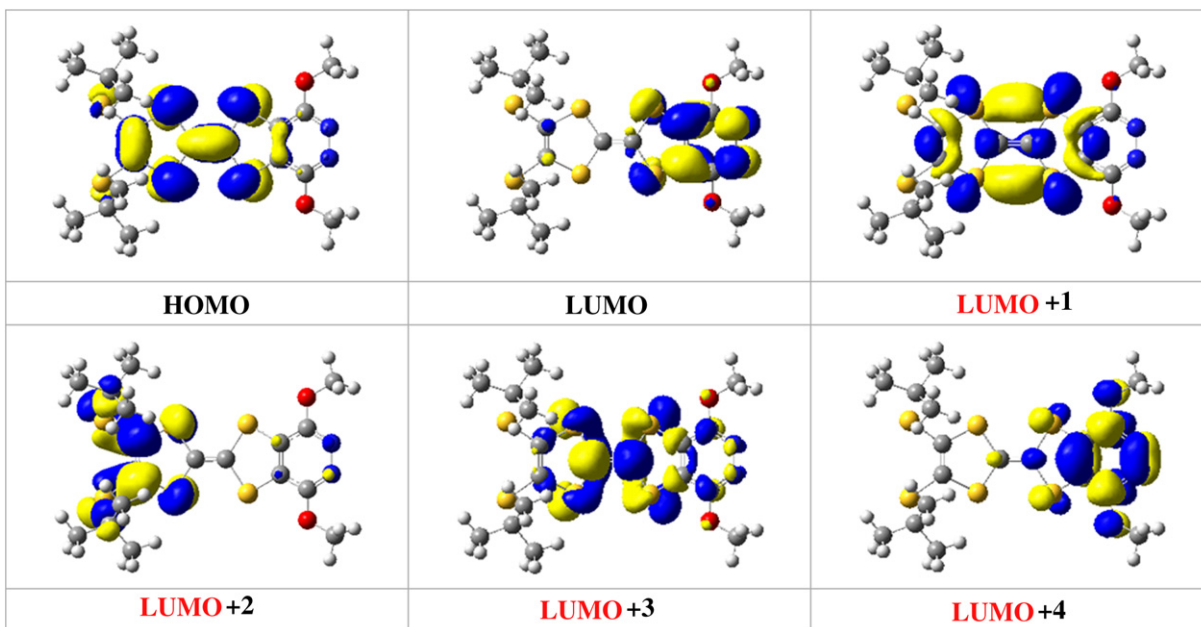


Fig. 5. Electron density contours (0.03 a.u.) calculated for the frontier orbital of molecule **12** at MPWPW91/TZVP level in chloroform.

### 3. Conclusion

In conclusion, we have synthesized a series donor–acceptor type pyridazine–TTF conjugates in which pyridazine ring part annulated directly to a TTF part. The studies on absorption spectra suggest the intramolecular charge transfer interaction between TTF and pyridazine parts in ground states, which is rationalized on the basis of density functional theory. Their HOMO energy levels and  $E_g^{\text{opt}}$  values were estimated to be  $-4.88$  to  $-5.07$  eV from cyclic voltammetry and  $2.43$ – $2.79$  eV from the absorption spectra, respectively. These results suggest that the present conjugates can be considered as candidates for hole transporting organic materials, such as semiconducting applications.

### 4. Experimental section

#### 4.1. Materials and apparatus

Commercially available compounds were used without further purification. Solvents were dried according to standard procedures. Compound **1**,<sup>14</sup> **2**,<sup>15</sup> **4**,<sup>16</sup> and **6**<sup>17</sup> were synthesized according to the reported procedures. All reactions were magnetically stirred and monitored by thin-layer chromatography (TLC) using QingDao GF<sub>254</sub> silica gel coated plates. UV–vis spectra were recorded with a Shimadzu UV-2550 spectrophotometer. NMR spectra were recorded on a Bruker AV-300 Spectrometer (300 MHz for <sup>1</sup>H and 75 MHz for <sup>13</sup>C), and chemical shifts were referenced relative to tetramethylsilane ( $\delta_{\text{H}}/\delta_{\text{C}}=0$ ). IR spectra were recorded on a Shimadzu FT-IR Prestige-21 instrument (KBr pressed disc method). Cyclic voltammetric studies were carried out on a Potentiostat/Galvanostat 273A instrument in CH<sub>2</sub>Cl<sub>2</sub>/CH<sub>3</sub>CN (1:1,  $c=1 \times 10^{-3}$  M) and 0.1 M Bu<sub>4</sub>PF<sub>6</sub> as the supporting electrolyte and scan rate is 100 mV S<sup>-1</sup>. Counter and Working electrodes were made of Pt and Glass-Carbon, respectively, and the reference electrode was calomel electrode (Ag/AgCl). MALDI-TOF mass data were obtained by a Shimadzu AXIMA-CFR™ plus mass spectrometry, using a 1, 8, 9-anthracenetriol (DITH) matrix.

#### 4.2. Synthesis

**4.2.1. Bis(3,6-dioxypyridazino[4,5-d])tetrathiafulvalene (5).** A mixture of **4** (95 mg, 0.219 mmol) and hydrazine hydrate (3 mL) in EtOH

(15 mL) was refluxed for 4 h. After cooling, the precipitate was filtered off and was washed by EtOH to give **5** (60 mg, 73.7%), Mp  $>290$  °C; IR (cm<sup>-1</sup>): 3182  $\nu$  (N–H), 1658  $\nu$  (amide C=O); MS (ESI)  $m/z$ : 371.0 ([M–H]<sup>-</sup>, 100).

**4.2.2. 2-(4,5-Bis(butylthio)-1,3-dithiol-2-ylidene)-5,6-dihydro-[1,3]dithiolo[4,5-d]pyridazine-4,7-dione (7).** A mixture of **6** (500 mg, 1.212 mmol) and hydrazine hydrate (5 mL) in EtOH (45 mL) was refluxed for 4 h. After cooling, the precipitate was filtered off and was washed with EtOH. The solid was recrystallized from DMF to give **7** as a red prisms (245.6 mg, 53%). Mp 209–210 °C; <sup>1</sup>H NMR (300 MHz, DMSO-*d*<sub>6</sub>):  $\delta$  2.87 (t,  $J=6.90$  Hz, 4H), 1.56–1.48 (m, 4H), 1.42–1.20 (m, 4H), 0.87 (t,  $J=7.20$  Hz, 6H); <sup>13</sup>C NMR (75 MHz, DMSO-*d*<sub>6</sub>):  $\delta$  153.00, 136.80, 127.74, 110.56, 34.67, 31.56, 21.37, 14.62; UV–vis (DMSO)  $\lambda$  (nm) ( $\epsilon$  L mol<sup>-1</sup> cm<sup>-1</sup>): 306 (15,460, sh), 322 (17,420), 387 (4280); IR (cm<sup>-1</sup>): 3165  $\nu$  (NH), 1647  $\nu$  (C=O); MS (ESI)  $m/z$ : 462.9 ([M–H]<sup>-</sup>, 100); Anal. Calcd for C<sub>16</sub>H<sub>20</sub>N<sub>2</sub>O<sub>2</sub>S<sub>6</sub>: C, 41.35; H, 4.34; N, 6.03. Found C, 41.56; H, 4.30; N, 5.99.

**4.2.3. 2-(4,5-Bis(butylthio)-1,3-dithiol-2-ylidene)-7-methoxy-[1,3]dithiolo[4,5-d]pyridazin-4(5H)-one (8).** A mixture of **7** (100 mg, 0.2152 mmol) and K<sub>2</sub>CO<sub>3</sub> (29.74 mg, 0.22 mmol) in DMF (20 mL) was stirred at room temperature for 30 min, then MeI (13.4  $\mu$ L, 0.22 mmol) was added. The mixture was stirred for 2 h and was monitored by TLC. Upon completion, the solution was evaporated in vacuo to dryness. The crude product was purified by column chromatography on silica gel using EtOAc/petroleum ether (v/v, 1:5) as the eluant to give a yellow solid. Recrystallization of the solid from DMF gave **8** as a yellow powder (58.6 mg, 57%). Mp 183–184 °C; <sup>1</sup>H NMR (300 MHz, CDCl<sub>3</sub>):  $\delta$  11.22 (br, 1H, NH), 3.89 (s, 3H), 2.84 (t,  $J=7.26$  Hz, 4H), 1.67–1.58 (m, 4H), 1.51–1.39 (m, 4H), 0.94 (t,  $J=7.29$  Hz, 6H); <sup>13</sup>C NMR (75 MHz, CDCl<sub>3</sub>):  $\delta$  155.43, 148.64, 139.34, 134.29, 128.40, 127.62, 115.23, 107.23, 55.11, 36.12, 31.75, 21.64, 13.58; UV–vis (CHCl<sub>3</sub>)  $\lambda$  (nm) ( $\epsilon$  L mol<sup>-1</sup> cm<sup>-1</sup>): 306 (16,268, sh), 322 (18,440), 430 (1640); IR (cm<sup>-1</sup>): 3128  $\nu$  (NH), 1653  $\nu$  (C=O); MS (MALDI-TOF):  $m/z$  479.7 ([M+H]<sup>+</sup>, 100); Anal. Calcd for C<sub>17</sub>H<sub>22</sub>N<sub>2</sub>O<sub>2</sub>S<sub>6</sub>: C, 42.65; H, 4.63; N, 5.85. Found C, 42.56; H, 4.41; N, 5.80.

**4.2.4. 2-(4,5-Bis(butylthio)-1,3-dithiol-2-ylidene)-7-methoxy-5-methyl-[1,3]dithiolo[4,5-d]pyridazin-4(5H)-one (9).** A mixture of **7** (50 mg, 0.11 mmol) and K<sub>2</sub>CO<sub>3</sub> (32.7 mg, 0.24 mmol) in DMF (10 mL)

was stirred at room temperature for 30 min, then MeI (14.7  $\mu\text{L}$ , 0.24 mmol) was added. The mixture was stirred and was monitored by TLC. Upon completion, the solution was evaporated in vacuo to dryness. The crude product was purified by column chromatography on silica gel using EtOAc/petroleum ether (v/v, 1:5) as the eluant to give a yellow solid. Recrystallization of the solid from hexane gave **9** as a yellow powder (51.1 mg, 96%). Mp 99–100 °C;  $^1\text{H NMR}$  (300 MHz,  $\text{CDCl}_3$ ):  $\delta$  3.87 (s, 3H), 3.65 (s, 3H), 2.85–2.79 (m, 4H), 1.67–1.56 (m, 4H), 1.50–1.38 (m, 4H), 0.93 (t,  $J=7.5$  Hz, 6H);  $^{13}\text{C NMR}$  (75 MHz,  $\text{CDCl}_3$ ):  $\delta$  153.79, 147.12, 140.17, 132.44, 128.64, 127.60, 114.53, 108.33, 55.08, 39.10, 36.28, 31.98, 21.81, 13.76; UV–vis ( $\text{CHCl}_3$ )  $\lambda$  (nm) ( $\epsilon$   $\text{L mol}^{-1} \text{cm}^{-1}$ ): 307 (18,300, sh), 323 (21,660), 432 (1840); IR ( $\text{cm}^{-1}$ ): 1647  $\nu$  (C=O), 1578  $\nu$  (C=N); MS (MALDI-TOF):  $m/z$  491.8 ( $\text{M}^+$ , 100); Anal. Calcd for  $\text{C}_{18}\text{H}_{24}\text{N}_2\text{O}_2\text{S}_6$ : C, 43.87; H, 4.91; N, 5.68. Found C, 44.00; H, 4.61; N, 5.72.

**4.2.5. 2-(4,5-Bis(butylthio)-1,3-dithiol-2-ylidene)-7-oxo-6,7-dihydro-[1,3]dithiolo[4,5-d]pyridazin-4-yl acetate (10).** A mixture of **7** (26.2 mg, 0.056 mmol), acetyl chloride (1 mL), and dry triethylamine (0.6 mL) in dry  $\text{CH}_2\text{Cl}_2$  (3 mL) was stirred at room temperature for 2 h under  $\text{N}_2$ . Then the solution was evaporated in vacuo to dryness. The crude product was purified by column chromatography on silica gel using EtOAc/petroleum ether (v/v, 1:2) as the eluant to give a red solid. The solid was recrystallized from acetonitrile to give **10** as red needles (10.6 mg 37%). Mp 165–166 °C;  $^1\text{H NMR}$  (300 MHz,  $\text{CDCl}_3$ ):  $\delta$  11.18 (br, 1H, NH), 2.83 (t,  $J=6.0$  Hz, 4H), 2.34 (s, 3H), 1.67–1.57 (m, 4H), 1.50–1.38 (m, 4H), 0.95 (t,  $J=7.20$  Hz, 6H).  $^{13}\text{C NMR}$  (75 MHz,  $\text{CDCl}_3$ ):  $\delta$  167.14, 155.18, 142.04, 140.91, 137.01, 128.89, 127.53, 117.02, 105.01, 36.26, 31.86, 21.70, 20.54, 13.65; UV–vis ( $\text{CHCl}_3$ )  $\lambda$  (nm) ( $\epsilon$   $\text{L mol}^{-1} \text{cm}^{-1}$ ): 307 (17,440, sh), 322 (18,640), 443 (1640); IR ( $\text{cm}^{-1}$ ): 1780  $\nu$  (ester C=O), 1649 (amide C=O), 1170  $\nu$  (C–O); MS (MALDI-TOF):  $m/z$  505.8 ( $\text{M}^+$ , 100); Anal. Calcd for  $\text{C}_{18}\text{H}_{22}\text{N}_2\text{O}_3\text{S}_6$ : C, 42.66; H, 4.38; N, 5.53. Found C, 43.00; H, 4.50; N, 5.63.

**4.2.6. 2-(4,5-Bis(butylthio)-1,3-dithiol-2-ylidene)-4,7-dichloro-[1,3]dithiolo[4,5-d]pyridazine (11).** A mixture of **2** (208 mg, 0.45 mmol) in neat  $\text{POCl}_3$  (5 mL) was refluxed overnight. After cooling, the excess  $\text{POCl}_3$  was removed under reduced pressure. The residual mixture was poured into water and extracted by  $\text{CH}_2\text{Cl}_2$ , the organic layer was separated, dried over anhydrous magnesium sulfate, and concentrated. The crude product was purified by column chromatography on silica gel using EtOAc/petroleum ether (v/v, 1:9) as the eluant to give a red solid. Recrystallization of the solid from hexane gave **11** as a red needles (201.7 mg, 90%). Mp 92–93 °C;  $^1\text{H NMR}$  (300 MHz,  $\text{CDCl}_3$ ):  $\delta$  2.84 (t,  $J=7.2$  Hz, 4H), 1.65–1.58 (m, 4H), 1.49–1.41 (m, 4H), 0.94 (t,  $J=7.3$  Hz, 6H);  $^{13}\text{C NMR}$  (75 MHz,  $\text{CDCl}_3$ ):  $\delta$  146.84, 142.58, 128.34, 120.37, 101.05, 36.40, 31.92, 21.81, 13.79; UV–vis ( $\text{CHCl}_3$ )  $\lambda$  (nm) ( $\epsilon$   $\text{L mol}^{-1} \text{cm}^{-1}$ ): 316 (16,420), 355 (7,080, sh), 437 (1600); IR ( $\text{cm}^{-1}$ ): 1485  $\nu$ , 1267  $\nu$  (aromatic heterocycle); MS (MALDI-TOF):  $m/z$  500.1 ( $\text{M}^+$ , 100); Anal. Calcd for  $\text{C}_{16}\text{H}_{18}\text{Cl}_2\text{N}_2\text{S}_6$ : C, 38.31; H, 3.62; N, 5.58. Found C, 39.00; H, 3.61; N, 5.56.

**4.2.7. 2-(4,5-Bis(butylthio)-1,3-dithiol-2-ylidene)-4,7-dimethoxy-[1,3]dithiolo[4,5-d]pyridazine (12).** Compound **11** (63.8 mg, 0.13 mmol) was added to solution of sodium (640 mg) in dry methanol (10 mL) and THF (5 mL). The reaction mixture was refluxed overnight. After cooling, the solvent was removed under reduced pressure. The solid residue was extracted by EtOAc and washed with water, the organic layer was dried over anhydrous magnesium sulfate, and concentrated. The crude product was purified by column chromatography on silica gel using EtOAc/petroleum ether (v/v, 1:5) as the eluant to give an orange solid. Recrystallization of the solid from hexane gave **12** as a red prism (30.2 mg, 48%). Mp 100–101 °C;  $^1\text{H NMR}$  (300 MHz,  $\text{CDCl}_3$ ):  $\delta$  4.13 (s,

6H), 2.86 (t,  $J=7.2$  Hz, 4H), 1.65–1.58 (m, 4H), 1.49–1.46 (m, 4H), 0.96 (t,  $J=7.3$  Hz, 6H);  $^{13}\text{C NMR}$  (75 MHz,  $\text{CDCl}_3$ ):  $\delta$  156.31, 131.05, 128.13, 115.25, 100.18, 55.36, 31.95, 21.83, 13.79; UV–vis ( $\text{CHCl}_3$ )  $\lambda$  (nm) ( $\epsilon$   $\text{L mol}^{-1} \text{cm}^{-1}$ ): 305 (21,460, sh), 319 (22,500), 404 (2460); IR ( $\text{cm}^{-1}$ ): 1572  $\nu$ , 1466  $\nu$ , 1373  $\nu$  (aromatic heterocycle), 1039 (C–O); MS (MALDI-TOF):  $m/z$  492.1 ( $\text{M}^+$ , 100); Anal. Calcd for  $\text{C}_{18}\text{H}_{24}\text{N}_2\text{O}_2\text{S}_6$ : C, 43.87; H, 4.91; N, 5.68. Found C, 44.01; H, 4.78; N, 5.66.

**4.2.8. 2-(4,5-Bis(butylthio)-1,3-dithiol-2-ylidene)-4,7-diphenoxy-[1,3]dithiolo[4,5-d]pyridazine (13).** A mixture of **11** (32.2 mg, 0.06 mmol), NaH (3.4 mg, 0.14 mmol), and phenol (13.3 mg, 0.14 mmol) in DMF (5 mL) was stirred at room temperature for 1 h. The mixture was poured into EtOAc and washed with water. The organic layer was dried over anhydrous magnesium sulfate, and concentrated. The crude product was purified by column chromatography on silica gel using EtOAc/petroleum ether (v/v, 1:9) as the eluant to give a yellow solid. Recrystallization of the solid from hexane gave **13** as an orange fine needle (25.3 mg, 64%). Mp 102–103 °C;  $^1\text{H NMR}$  (300 MHz,  $\text{CDCl}_3$ ):  $\delta$  7.40–7.34 (m, 4H), 7.22–7.18 (m, 6H), 2.86 (t,  $J=7.2$  Hz, 4H), 1.70–1.60 (m, 4H), 1.53–1.41 (m, 4H), 0.95 (t,  $J=7.3$  Hz, 6H);  $^{13}\text{C NMR}$  (75 MHz,  $\text{CDCl}_3$ ):  $\delta$  156.84, 153.13, 132.64, 129.77, 128.20, 125.71, 121.36, 116.75, 107.11, 36.35, 31.96, 21.84, 13.81; UV–vis ( $\text{CHCl}_3$ )  $\lambda$  (nm) ( $\epsilon$   $\text{L mol}^{-1} \text{cm}^{-1}$ ): 308 (18,560, sh), 321 (20,000), 415 (1760); IR ( $\text{cm}^{-1}$ ): 1568  $\nu$ , 1489  $\nu$ , 1379 (aromatic heterocycle), 1209 (C–O); MS (MALDI-TOF):  $m/z$  617.0 ( $[\text{M}+\text{H}]^+$ , 100); Anal. Calcd for  $\text{C}_{28}\text{H}_{28}\text{N}_2\text{O}_2\text{S}_6$ : C, 54.51; H, 4.57; N, 4.54. Found C, 54.52; H, 4.58; N, 4.60.

### 4.3. X-ray crystal structure determination

X-ray diffraction experiment was performed with a Rigaku/MSC mercury diffractometer with graphite monochromated Mo  $K\alpha$  radiation ( $\lambda=0.71073$  E) at 293 K. Empirical absorption corrections based on equivalent reflections were applied. The crystal structures were solved by direct method and refined by full matrix least squares fitting on  $F^2$  using the SHELXTL-97 software. All non-hydrogen atoms were refined with anisotropic thermal parameters. Crystallography data has been deposited to the Cambridge Crystallography Data Centre with deposition number of 846983–846986 for **7**, **11**–**13**. Copies of this information may be obtained free of charge from The CCDC, 12 Union road, Cambridge CB2 1EZ, UK (fax: +44 1223 336033; e-mail: [deposit@ccdc.cam.ac.uk](mailto:deposit@ccdc.cam.ac.uk) or <http://www.ccdc.cam.ac.uk>).

### Acknowledgements

The authors acknowledge financial support from the National Natural Science Foundation of China (grant No.21062022) and the Specialized Research Fund for the Doctoral Program of Higher Education (Grant No. 20102201110001).

### Supplementary data

Supplementary data related to this article can be found online at [doi:10.1016/j.tet.2011.12.034](http://dx.doi.org/10.1016/j.tet.2011.12.034).

### References and notes

- (a) Andrieux, A.; Duromre, C.; Jérôme, D.; Bechgaard, K. *J. Phys., Lett.* **1979**, *40*, 381–384; (b) Lyskawa, J.; LeDerf, F.; Levillain, E.; Mazari, M.; Salle, M.; Dubois, L.; Viel, P.; Bureau, C.; Palacin, S. *J. Am. Chem. Soc.* **2004**, *126*, 12194–12195; (c) Wang, L.; Zhang, B.; Zhang, J. *Inorg. Chem.* **2006**, *45*, 6860–6863; (d) Mas-Torrent, M.; Rovira, C. *Chem. Commun.* **2006**, 433–436; (e) Martín, N.; Sánchez, L.; Herranz, M. Á.; Illesca, B.; Guldí, D. M. *Acc. Chem. Res.* **2007**, *40*, 1015–1024; (f) Mas-Torrent, M.; Hadley, P.; Bromley, S. T.; Ribas, X.; Tarres, J.; Mas, M.; Molins, E.; Veciana, J.; Rovira, C. *J. Am. Chem. Soc.* **2004**, *126*, 8546–8553.
- (a) Otsubo, T.; Aso, Y.; Takimiya, K. *Adv. Mater.* **1996**, *8*, 203–211; (b) Bryce, M. R. *J. Mater. Chem.* **1995**, *5*, 1481–1496; (c) Garin, J. *Adv. Heterocycl. Chem.* **1995**, *62*,

- 249–304; (d) Adam, M.; Müllen, K. *Adv. Mater.* **1994**, *6*, 439–459; (e) Schukat, G.; Fanghänel, E. *Sulfur Rep.* **1996**, *18*, 1–294; (f) Andreu, R.; Barberá, J.; Garín, J.; Orduna, J.; Serrano, J. L.; Sierra, T.; Leriche, P.; Sallé, M.; Riou, A.; Jubault, M.; Gorgues, A. *J. Mater. Chem.* **1998**, *8*, 881–887.
3. Naraso; Nishida, J.; Ando, S.; Yamaguchi, J.; Itaka, K.; Koinuma, H.; Tada, H.; Tokito, S.; Yamashita, Y. *J. Am. Chem. Soc.* **2005**, *127*, 10142–10143.
4. (a) Kini, A. M.; Geiser, U.; Wang, H. H.; Carlson, K. D.; Williams, J. M.; Kwok, W. K.; Vandervoort, K. G.; Thompson, J. E.; Stupka, D. L.; Jung, D.; Whangbo, M.-H. *Inorg. Chem.* **1990**, *29*, 2555–2557; (b) Lerstrup, K.; Talham, D.; Bloch, A.; Cowan, D. *J. Chem. Soc., Chem. Commun.* **1982**, 336–337; (c) Siquot, Y.; Frère, P.; Nozdryn, T.; Cousseau, J.; Sallé, M.; Jubault, M.; Orduna, J.; Garín, J.; Gorgues, A. *Tetrahedron Lett.* **1997**, *38*, 1919–1922; (d) Shu, P.; Chiang, L.; Emge, T.; Holt, D.; Kistenmacher, T.; Lee, M.; Stokes, J.; Poehler, T.; Bloch, A.; Cowan, D. *J. Chem. Soc., Chem. Commun.* **1981**, 920–921; (e) Ketcham, R.; Hörnfeldt, A.-B.; Gronowitch, S. *J. Org. Chem.* **1984**, *49*, 1117–1119; (f) Guégano, X.; Kanibolotsky, A. L.; Blum, C.; Mertens, S. F. L.; Liu, S.-X.; Neels, A.; Hans Hagemann, H.; Peter, J.; Skabara, P. J.; Leutwyler, S.; Wandlowski, T.; Hauser, A.; Decurtins, S. *Chem.—Eur. J.* **2009**, *15*, 63–66; (g) Jia, C. Y.; Liu, S.-X.; Tanner, C.; Leiggenger, C.; Neels, A.; Sanguinet, L.; Levillain, E.; Leutwyler, S.; Hauser, A.; Decurtins, S. *Chem.—Eur. J.* **2007**, *13*, 3804–3812; (h) Wu, J. C.; Dupont, N.; Liu, S.-X.; Neels, A.; Hauser, A.; Decurtins, A. *Chem.—Asian J.* **2009**, *4*, 392–399; (i) Neilands, O.; Belyakov, S.; Vija Tlika, V.; Edžina, A. *J. Chem. Soc., Chem. Commun.* **1995**, 325–326; (j) Neilands, O.; Tilika, V.; Sudmale, I.; Grigorjeva, I.; Edžina, A.; Fonavs, E.; Muzikante, I. *Adv. Mater. Opt. Electron.* **1997**, *7*, 93–97.
5. (a) Gorgues, A.; Batail, P.; Le Coq, A. *J. Chem. Soc., Chem. Commun.* **1983**, 405–406; (b) Papavassiliou, G. C.; Yiannopoulos, S. Y.; Zameounisi, J. S. *Mol. Cryst. Liq. Cryst.* **1985**, *120*, 333–336; (c) Salle, M.; Gorgues, A.; Jubault, M.; Boubekeur, K.; Batail, P. *Tetrahedron* **1992**, *48*, 3081–3090.
6. Castle, R. N. *Pyridazines*; Wiley-Interscience: New York, NY, 1973.
7. Kaner, R. B.; Porter, S. J.; Nairns, D. P.; MacDiarmid, A. G. *J. Chem. Phys.* **1989**, *90*, 5102–5107.
8. Egbe, D. A. M.; Cornelia, B.; Nowotny, J.; Gunther, W.; Klemm, E. *Macromolecules* **2003**, *36*, 5459–5469.
9. Chang, C. J.; Yang, C. H.; Chen, K.; Chi, Y.; Shu, C. F.; Ho, M. L.; Yeh, Y. S.; Chou, P. T. *Dalton Trans.* **2007**, 1881–1890.
10. Jeppesen, J. O.; Takimiya, K.; Jensen, F.; Brimert, T.; Nielsen, K.; Thorup, N.; Becher, J. *J. Org. Chem.* **2000**, *65*, 5794–5805.
11. Guerro, M.; Dam, T. U.; Bakhta, S.; Kolli, B.; Roisnel, T.; Lorcy, D. *Tetrahedron* **2011**, *67*, 3427–3433.
12. Murphy, A. R.; Frechet, J. M. J. *Chem. Rev.* **2007**, *107*, 1066–1096.
13. Nishida, N. J.; Kumaki, D.; Tokito, S.; Yamashita, Y. *J. Am. Chem. Soc.* **2006**, *128*, 9598–9599.
14. Melby, L. R.; Hartzler, H. D.; Sheppard, W. A. *J. Org. Chem.* **1976**, *41*, 2855–2860.
15. Chen, T.; Wang, C. L.; Cong, Z. Q.; Yin, B. *Z. Heterocycles* **2005**, *65*, 187–193.
16. Toplak, R.; Benard-Rocherulle, P.; Lorcy, D. *Tetrahedron Lett.* **2002**, *43*, 3879–3882.
17. Hasegawa, M.; Takano, J.; Enozawa, H.; Kuwatani, Y.; Iyoda, M. *Tetrahedron Lett.* **2004**, *45*, 4109–4112.